

# COMPARISON BETWEEN TWO ITERATIVE SCHEMES FOR THE ONE DIMENSIONAL MARCHENKO EQUATION

*J. Magalhães, J. Schleicher, and A. Novais*

**email:** *candido.magalhaes@hotmail.com, js@ime.unicamp.br*

**keywords:** *Marchenko, inversion, one-way*

## ABSTRACT

*Solving the 1D Marchenko equation by means of iterative schemes allows to obtain the redatumed Green's function at an arbitrary focusing position. We compare two algorithms proposed in the literature to achieve this goal. Our careful implementations have demonstrated that while kinematically equivalent, these algorithms lead not to fully identical results. While the older algorithm is somewhat faster, the newer one provides superior amplitudes and separates up and downgoing components of the recovered Green's function.*

## INTRODUCTION

The one dimensional Marchenko equation is a well-known integral equation that solves the inverse scattering problem for a constant background medium with some localized scattering region (Burrige, 1980; Aktosun, 1987).

Rose (2002) developed an iterative way to construct a particular initial waveform in such a way that it reduces to a  $\delta$ -pulse at a particular time, called the focusing time. He also proved that by constructing this waveform we are solving the Marchenko equation.

Broggini and Snieder (2012) demonstrated that combining the solution of this scheme with its time-reversed version allows to obtain the redatumed Green's function at a focusing position without knowledge of the velocity profile. Wapenaar et al. (2013) extended this principle to three dimensions and derived, via Green's theorem, the coupled Marchenko equations, which constitute a relationship between the Green's function and the fundamental solutions of the inverse scattering problem. van der Neut et al. (2015) later developed an alternative iterative scheme to solve the coupled Marchenko equations. His scheme bears some similarity to Rose's iterative scheme.

The coupled Marchenko equations can be used in several seismic applications, ranging from redatuming (Meles et al., 2016; Cui et al., 2018), imaging (Wapenaar et al., 2014; Singh et al., 2015; Meles et al., 2018), velocity analysis (Mildner et al., 2017) to inversion (Semih, 2018).

In this paper, we present a derivation of the one dimensional coupled Marchenko equations, discuss the differences of the two algorithms, and numerically compare the two schemes in two different velocity models.

## THEORY

The Marchenko Integral Equation is a relation that attempts to solve the perturbed Helmholtz equation, also known as time-independent Schrödinger equation (Lamb, 1980). In a one-dimensional medium, it is given by

$$\frac{d^2}{dx^2} \hat{u}(x, \omega) + \frac{\omega^2}{c_0^2} [1 + \alpha(x)] \hat{u}(x, \omega) = 0. \quad (1)$$

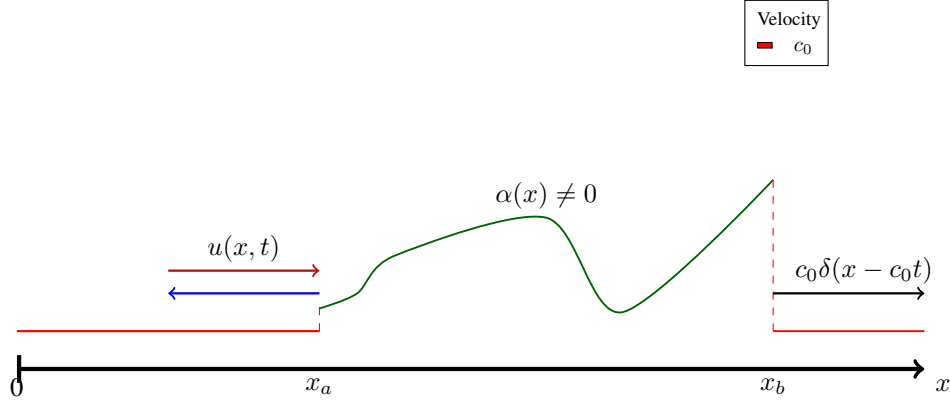


**Figure 1:** Right-going fundamental solution of equation (1). A wavefield  $u^+(x, t)$  consisting of a  $\delta$ -pulse and a coda incides from the left (red arrow) on the localized scattering region ( $\alpha(x) \neq 0$ ), producing a scattered wavefield  $u^-(x, t)$  (blue arrow) propagating to the left and a  $\delta$ -pulse (black arrow) propagating to the right. All right-going scattered events produced by the incident  $\delta$ -pulse are canceled by the coda.

Here,  $\hat{u}(x, \omega)$  is the fundamental solution for this type of problem,  $c_0$  is the background wave velocity (assumed to be constant) and  $\alpha(x)$  is the medium perturbation, also called the localized scattering potential.

It is well-known that a second-order differential equation like (1) has two fundamental solutions. One example of such a pair of fundamental solutions consists of a right-going waveform incident from the left-hand side, crossing the scattering region in such a way that on its right-hand side only a  $\delta$ -pulse propagates to the right, and a symmetrically constructed left-going waveform (Lamb, 1980). For reasons of brevity, here we consider only the right-going fundamental solution. This fundamental solution can be represented in the time domain as

$$u(x, t) = c_0 \delta(x - c_0 t) + c_0 H(c_0 t - x) \mathbf{C}(x, c_0 t), \quad (2)$$

where  $\mathbf{C}(x, c_0 t)$  is the so-called coda. A waveform  $u(x, t)$  of this form is the searched-for fundamental solution of equation (1) if, when the coda passes through the scattering region, it cancels all other left-to-right going pulses created by the leading  $\delta$ -pulse, such that to the right of the scattering region, only a  $\delta$ -pulse remains with the same propagation direction of  $u$  (Figure 1).

Wapenaar et al. (2013) denominate the fundamental solution  $u(x, t)$  focusing function, because to the right of the scattering region, it consists of a right-going  $\delta$ -pulse only. We can think of it as focusing at time  $t = 0$  at some focusing point  $x_f$  to the right of the perturbed region. For this reason, we can relate it with the Green's function  $\mathcal{G}(x, \omega; x_s)$ , i.e., the solution of the Helmholtz equation with a point source,

$$\frac{d^2}{dx^2} \hat{\mathcal{G}}(x, \omega; x_s) + \frac{\omega^2}{c(x)^2} \hat{\mathcal{G}}(x, \omega; x_s) = \delta(x - x_s), \quad (3)$$

where  $x_s$  denotes the source point. Actually, in a homogeneous 1D unbounded medium, the solution to equation (3) is (Bleistein et al., 2001)

$$\mathcal{G}(x, t; x_s) = \frac{c_0}{2} H(c_0 t - |x - x_s|). \quad (4)$$

However, in our numerical solution, we want to see a propagating unitary pulse. Therefore, we consider a modified version of equation (3) with a time derivative and a normalization applied to the source term, i.e.,

$$\frac{d^2}{dx^2} \hat{G}(x, \omega; x_s) + \frac{\omega^2}{c(x)^2} \hat{G}(x, \omega; x_s) = 2i \frac{\omega}{c_0} \delta(x - x_s). \quad (5)$$

A comparison of equations (3) and (5) reveals that the functions  $\hat{G}$  and  $\hat{\mathcal{G}}$  relate to each other as

$$\hat{G} = 2i \frac{\omega}{c_0} \hat{\mathcal{G}}. \quad (6)$$

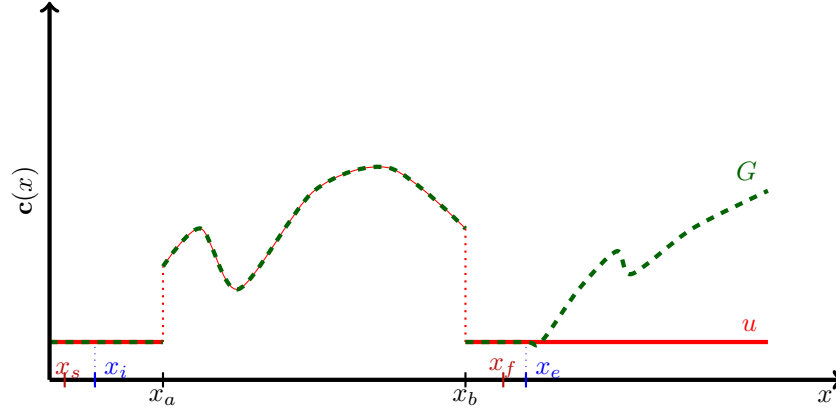


**Figure 2:** Velocity model for the two functions under consideration. Attention to the region where the velocity for both functions are equal.

To derive a relationship between the focusing function  $\hat{u}$  and the Green's function  $\hat{G}$ , we multiply equation (1) by  $\hat{G}(x, \omega; x_s)$ , and equation (5) by  $\hat{u}(x, \omega)$  and subtract the results. We then integrate the differences from a point  $x_i$  slightly beyond the source point  $x_s$  to a point  $x_e$  slightly beyond the desired focusing point  $x_f$  (see points  $x_i$  and  $x_e$  in Figure 2) and apply the 1D version of Green's theorem (see, e.g., Bleistein et al., 2001). In this way, in the limit of very small  $\epsilon$ , we find

$$\lim_{\epsilon \rightarrow 0^+} \left[ \left( \hat{G}^+ + \hat{G}^- \right) \frac{d}{dx} [\hat{u}^+ + \hat{u}^-] - (\hat{u}^+ + \hat{u}^-) \frac{d}{dx} [\hat{G}^+ + \hat{G}^-] \right] \Big|_{x_s+\epsilon}^{x_f+\epsilon} = 0, \quad (7)$$

where we have assumed that the velocity distribution  $c(x)$  in equation (3) equals the one in equation (1) within the interval  $(x_s, x_f)$  and that the velocity is constant in small vicinities of size  $\epsilon$  to the right of  $x_s$  and  $x_f$ , including points  $x_i$  and  $x_e$ , respectively. Moreover, we have written the involved wavefields as sums of their left-going (superscript  $-$ ) and right-going (superscript  $+$ ) components.

Using a high frequency approximation for both wavefields, we can show that at  $x_s$  and  $x_f$  (Wapenaar et al., 2013),

$$\hat{G}^- \frac{d}{dx} \hat{u}^- \approx \hat{u}^- \frac{d}{dx} \hat{G}^- \quad \text{and} \quad \hat{G}^+ \frac{d}{dx} \hat{u}^+ \approx \hat{u}^+ \frac{d}{dx} \hat{G}^+, \quad (8)$$

$$\hat{G}^- \frac{d}{dx} \hat{u}^+ \approx -\hat{u}^+ \frac{d}{dx} \hat{G}^- \quad \text{and} \quad \hat{G}^+ \frac{d}{dx} \hat{u}^- \approx -\hat{u}^- \frac{d}{dx} \hat{G}^+. \quad (9)$$

Thus, equation (7) simplifies to

$$\lim_{\epsilon \rightarrow 0^+} \left[ \hat{G}^+ \frac{d}{dx} \hat{u}^- + \hat{G}^- \frac{d}{dx} \hat{u}^+ \right] \Big|_{x=x_f+\epsilon} = - \lim_{\epsilon \rightarrow 0^+} \left[ \hat{u}^+ \frac{d}{dx} \hat{G}^- + \hat{u}^- \frac{d}{dx} \hat{G}^+ \right] \Big|_{x=x_s+\epsilon}. \quad (10)$$

Our fundamental solution  $u(x, t)$  has to satisfy some convenient constraints. We require it to pass at focusing point  $x_f$  at  $t = 0$ , which implies that it has to pass at  $x_s$  (the source injection position for  $G(x, t; x_s)$ ) at  $t = -t_f$ , where  $t_f$  is the one-way traveltime between  $x_s$  and  $x_f$ . Moreover, beyond  $x_f$ ,  $u^+$  is given, by construction, by a  $\delta$ -pulse and  $u^-$  vanishes. These requirements translate into the conditions

$$\frac{d}{dx} \hat{u}^-(x_f + \epsilon, \omega) = 0, \quad (11)$$

$$\frac{d}{dx} \hat{u}^+(x_f + \epsilon, \omega) = i \frac{\omega}{c_0} e^{i\omega\epsilon/c_0}. \quad (12)$$

Moreover, since the medium is assumed to be homogeneous to the left of  $x_s$ , the right-going part of  $G$  slightly to the right of  $x_s$  must still be equal to what it would be in a homogeneous medium. Thus, taking

the derivative and Fourier Transform of equation (4) and making use of equation (6), we find

$$\frac{d}{dx} \widehat{G}^+(x_s + \epsilon, \omega, x_s) = i \frac{\omega}{c_0} e^{i\omega\epsilon/c_0}. \quad (13)$$

Finally, the left-going part of the Green's function is related to the reflection response  $R(x_s, t, x_s)$  of the medium. Taking the spatial derivative of its Fourier transform, we therefore have

$$\frac{d}{dx} \widehat{G}^-(x_s + \epsilon, \omega, x_s) \approx -i \frac{\omega}{c_0} \widehat{R}(x_s + \epsilon, \omega; x_s), \quad (14)$$

where  $\widehat{R}(x, \omega; x_s)$  is the reflection response of the medium for the normalized source according to equation (5).

Substituting these boundary conditions in equation (10) and taking the limits results in the following time and frequency-domain expressions:

$$\widehat{G}^-(x_f, \omega; x_s) = \widehat{R}(x_s, \omega; x_s) \widehat{u}^+(x_s, \omega) - \widehat{u}^-(x_s, \omega), \quad (15)$$

$$G^-(x_f, t; x_s) = R(x_s, t; x_s) * u^+(x_s, t) - u^-(x_s, t). \quad (16)$$

The same procedure applied to the time reversed version of  $u$ , i.e., using the complex conjugate of equation (1), yields

$$\widehat{G}^+(x_f, \omega; x_s) = -\widehat{R}(x_s, \omega; x_s) \widehat{u}^{+*}(x_s, \omega) + \widehat{u}^{+*}(x_s, \omega), \quad (17)$$

$$G^+(x_f, t; x_s) = -R(x_s, t; x_s) * u^-(x_s, -t) + u^+(x_s, -t). \quad (18)$$

Expressions (15) and (17), or (16) and (18) in the time domain, are called the coupled Marchenko equations (Wapenaar et al., 2013).

### Broggini and Snieder's method

On the basis of the work of Rose (2002), Broggini and Snieder (2012) developed an iterative scheme that focuses an initial pulse at a prescribed time  $t_f$  using data recorded with a zero-offset configuration. To graphically demonstrate the underlying operations, we use the model depicted in Figure 3 with the focusing point at 4 km.

The procedure proposed by Rose (2002) consists in first injecting at  $x_s$  a known pulse  $Q(t) = q(t) \equiv \frac{2}{c(x_s)} \delta(t + t_f) \delta(x - x_s)$  shifted to  $-t_f$  and record the medium response  $S^0(x_s, t; x_s)$ . Because the solution of the one dimensional wave equation integrates the initial wavelet (since the Green's function is a Heaviside function), by injecting  $\frac{d}{dt} Q(t)$  the recorded wavefield will have the desired wavelet shape  $Q(t)$ . Second, to obtain the reflection response  $R^0(x_s, t; x_s)$  simply take the difference between the recorded wavefield at  $x_s$  and the injected pulse,

$$R^0(x_s, t; x_s) = S^0(x_s, t; x_s) - Q^0(t). \quad (19)$$

(Figure 4) shows this result for a model with two high-velocity zones between  $x_s$  and  $x_f$ .  $R^0(x_s, t; x_s)$  can be replaced by a recorded reflection response,  $R(x_s, t; x_s)$ , if available.

The third step consists of applying a window operator  $H(t_f - t)$  to the reflection response  $R^0(x_s, t; x_s)$  and reversing it in time. This time reversed version, called coda (Figure 5), is given by

$$coda^0(t) = R^0(x_s, -t; x_s) H(t_f + t). \quad (20)$$

Next, the injected pulse is updated by taking the difference between the initial wavelet  $Q^0(t)$  and the coda  $coda^0(t)$  to produce the new wavelet  $Q^1(t)$  (Figure 6). The procedure starts then over by injecting  $\frac{d}{dt} Q^1(t)$ , recording the new response  $R^1(x_s, t; x_s)$ , and calculating the new  $coda^1(t)$ . At each iteration,  $Q^k(t)$  is obtained by subtracting the coda from  $Q^0$ . The process continues iteratively  $k$  times until it reaches convergence to obtain  $Q^k(t)$ .

Broggini and Snieder (2012) showed that  $G(x_f, w; x_s)$  can be obtained by convolving the original seismic reflection response  $R(x_s, t; x_s)$  at  $x_s$  with the injected wavelet  $Q(t)$  as described above, i.e., after  $k$  iterations,  $u(x_s, t) = R(x_s, t; x_s) *_t Q^k(t)$  (Figure 7), and adding its time reversed version  $u(x_s, -t)$  (Figure 8(a)). Figure 7 shows the result of this procedure after four iterations. The algorithm is summarized in Table 1.

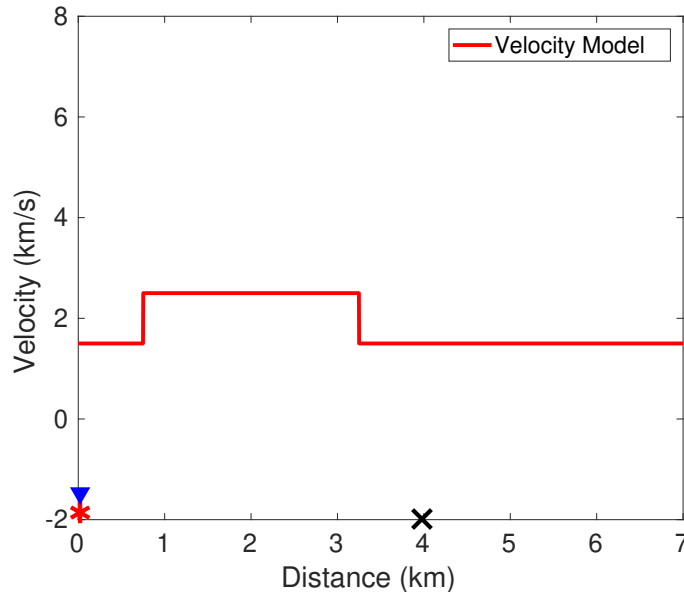


**Figure 3:** Velocity model with a high velocity zone (2.5 km/s). Markers denoted by a black cross, red asterisk, and blue triangle represents the chosen focusing point, source and observation point, respectively.

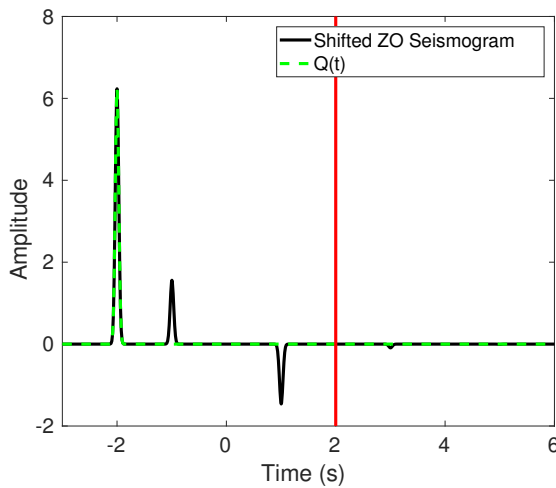


**Figure 4:** Broggini and Snieder's Algorithm: The Gaussian wavelet  $Q^0(t) = Q(t)$  simulating a  $\delta$ -pulse used at the first iteration (dashed green line) and the corresponding recorded seismogram  $S^0(x_s, t; x_s)$  (solid black line).

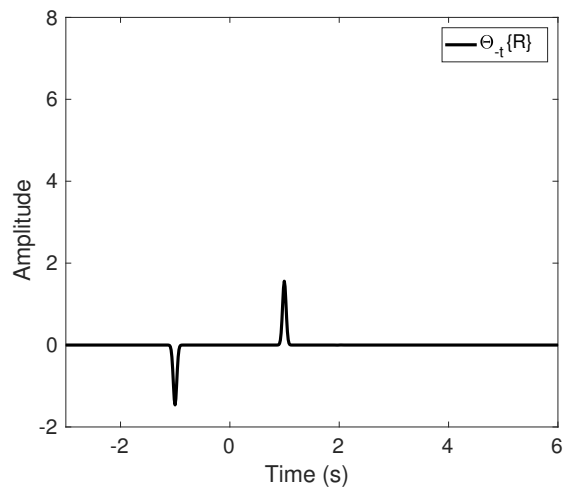


**Figure 5:** Broggini and Snieder's Algorithm: Time reversed and windowed reflection response at the first iteration,  $coda^0(t)$ , obtained according to equation (20).

**van der Neut's method**

For the coupled Marchenko equations, van der Neut et al. (2015) developed the following iterative scheme: First, think of  $u^+$  as composed of an initial unitary direct pulse  $u_d$  and a following coda corresponding to equation (2), i.e.,

$$u^+ = u_d + u_{coda} . \tag{21}$$

Note again that the designed focusing function is subject to some constraints:  $u_d$  has to pass at  $x_s$  at a specified focusing time  $-t_f$  so as to reach the focusing point  $x_f$  at  $t = 0$ . Hence, without any knowledge

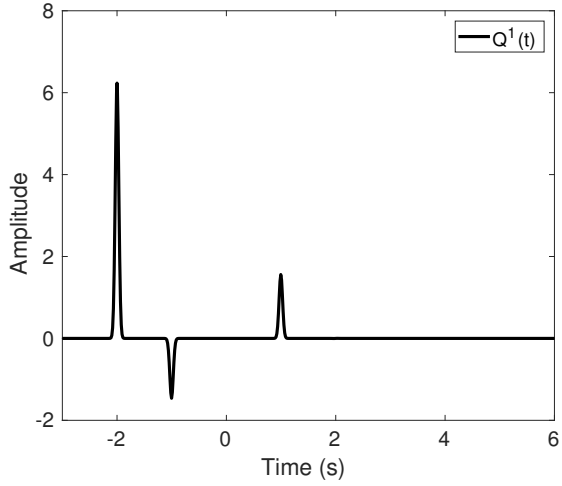


**Figure 6:** Wavelet  $Q^1(t)$  after first iteration update.

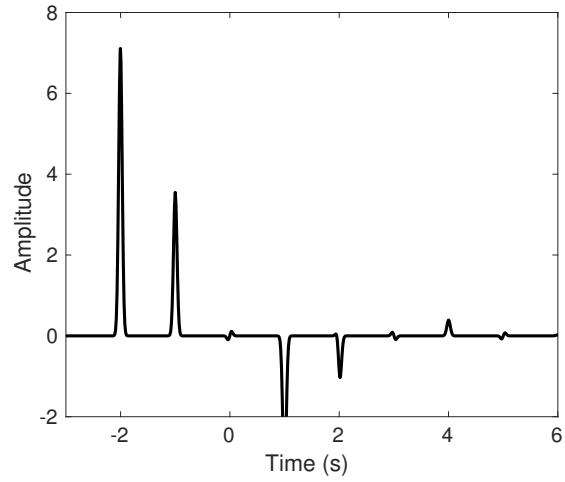


**Figure 7:** Seismogram recorded after 4 iterations, i.e., injecting  $\frac{d}{dt}Q^3(t)$ .

of the velocity model, the obtained Green's function will be simulated at an unknown position.

Consistent with the boundary conditions, design a window operator  $\Theta = H(tf - |t|)$ , that preserves the field between  $-t_f$  and  $t_f$ , and zeroes the field outside this interval. Windowing  $u^-$ ,  $u^+$ , and  $G$  results in

$$\Theta\{G\} = 0, \quad (22)$$

$$\Theta\{u^+\} = u_{coda}, \quad (23)$$

$$\Theta\{u^-\} = u^-. \quad (24)$$

It is important to recognize that there is no field registered before  $t_f$  at  $x_s$  because the Green's function localized at  $x_f$  is causal. Thus, masking the Green's function with  $\Theta$  gives zero. On the other hand, the leftward propagating part of  $u$  exists only within the time window between  $-t_f$  and  $t_f$ , so that it is not affected by the masking.

The masking of  $u^+$  in the prescribed two-way traveltime window ( $-t_f$  to  $t_f$ ) is done in such a way that the direct field  $u_d$  is removed, but all primaries and multiples that will possibly arrive at  $x_s$  are preserved. Using this window operator on the time domain coupled Marchenko equations yields

$$\Theta\{R(x_s, t; x_s) * u^+(x_s, t)\} = u^-(x_s, t), \quad (25)$$

$$\Theta\{R(x_s, t; x_s) * u^-(x_s, -t)\} = u_{coda}^+(x_s, -t). \quad (26)$$

The algorithm starts by setting  $u_{coda}^0 = 0$  and  $u_d^0 = \delta(c_0(t + t_f) - |x - x_s|)$  in the first iteration. The use of these initial values in equation (25) yields  $u^-$ , which, upon substitution in equation (26), provides  $u_{coda}^1$ . This iterative process can be repeated until it meets some convergence criterion. Upon reaching convergence,  $G^+$  and  $G^-$  are calculated by equations (16) and (18). Figure 8(b) shows the complete Green's function obtained with this iterative scheme. The algorithm is summarized in Table 2.

Figure 8 shows the redatumed Green's function for the velocity model depicted in Figure 3. The dashed black line represents the Finite-Differences reference solution with source position at the focusing point, i.e.,  $x_s = x_f$  recorded at position  $x_g = 0$ . The solid red line in Figures 8(a) and 8(b) represents the solution for the Broggini and Snieder's; and van der Neut's algorithms, respectively. We see that both algorithms produce an event at  $-t_f$ , though of different magnitude and that Broggini and Snieder's algorithm also produces some minor artifacts that are not present in the result of van der Neut's algorithm.

## NUMERICAL EXAMPLES

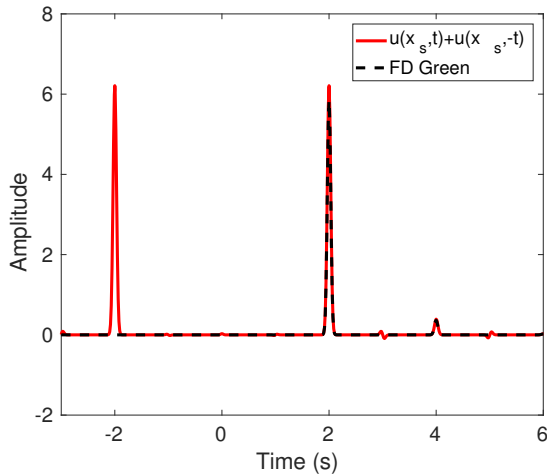
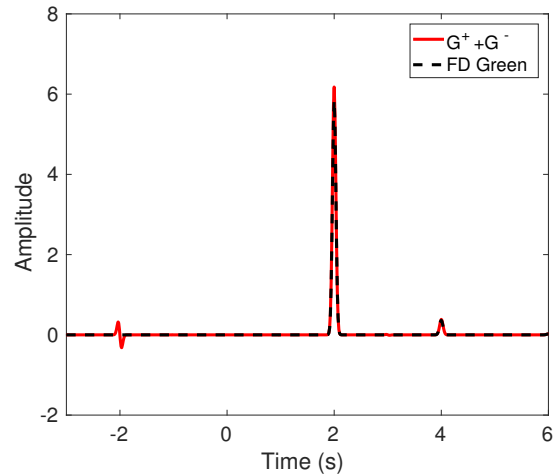
We performed numerical tests in two different velocity models, shown in Figure 9 both using a Ricker wavelet with unitary peak amplitude.

**Broggini and Snieder's Algorithm**

1.  $k \leftarrow 0$
2.  $Q^k(t) \leftarrow \delta(t + t_f)$
3. Inject  $Q^k$  and record  $S^k$  at  $x_s$
4.  $R^k \leftarrow S^k - Q^k$
5.  $coda^k \leftarrow R^k(-t)H(t_f + t)$
6.  $Q^{k+1}(t) \leftarrow Q^0 - coda^k$
7.  $k \leftarrow k + 1$ ;
8. If  $Q^k$  does not satisfy convergence criterion: Goto step 3
9. After convergence:  
Inject  $Q^k$  and record  $u(t)$
10.  $G^k \leftarrow u(t) + u(-t)$

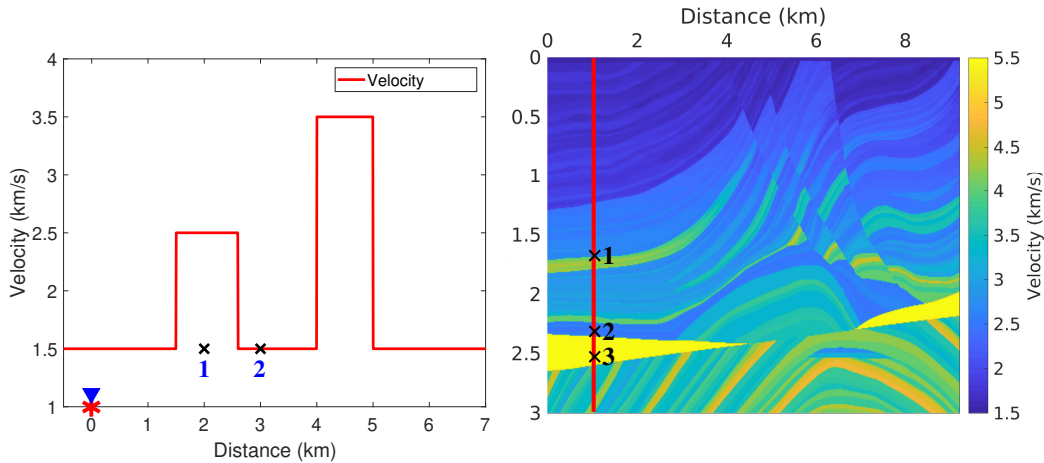
**van der Neut's Algorithm**

1.  $u_d(t) \leftarrow \delta(t + t_f)$
2.  $k \leftarrow 0$
3.  $u_{coda}^k \leftarrow 0$
4.  $u^{+k} \leftarrow u_d + u_{coda}^k$
5.  $u^{-k} \leftarrow \Theta\{R * u^{+k}\}$
6.  $u_{coda}^{+(k+1)}(x_s, -t) \leftarrow \Theta\{R * u^{-k}(-t)\}$
7.  $k \leftarrow k + 1$ ;
8. If  $u_{coda}^{+k}$  does not satisfy convergence criterion: Goto step 4
9. After convergence:  
 $G^{-k} \leftarrow R(t) * u^{+k}(t) - u^{-k}(t)$
10.  $G^{+k} \leftarrow -R(t) * u^{-k}(-t) + u^{+k}(-t)$
11.  $G^k \leftarrow G^{+k} + G^{-k}$

**Table 1:** Broggini and Snieder's Algorithm.**Table 2:** van der Neut's Algorithm.**(a)** Numerical result using Broggini and Snieder's iterative algorithm.**(b)** Numerical result using van der Neut's iterative algorithm based on the coupled Marchenko equations.**Figure 8:** Results for the focusing time  $t_f = 2$  s corresponding to  $x_f = 4$  km (black cross in Figure 3).

The first velocity model (Figure 9(a)) has two high velocity zones in a constant background velocity, and we chose two focusing points, being one inside the first high velocity zone where  $c(x_s) \neq c(x_{f1})$  and another one in between the two high velocity zones where  $c(x_s) = c(x_{f2})$ .

The second velocity model is a vertical profile from the Marmousi model extracted at lateral position  $x = 1$  km. We chose 3 focusing points at vertical positions  $z = 1.7$  km,  $z = 2.3$  km, and  $z = 2.5$  km, as shown in Figure 9(b).



(a) Two high velocity zones with constant background (b) Marmousi model. Red vertical line represents the vertical profile velocity. Black crosses markers are the chosen focusing and black crosses markers the chosen focusing points.

**Figure 9:** Two velocity models used in our numerical experiments.

### Simple model

Figures 10 and 11 compare the iterative solutions of Brogini and Snieder's scheme and van der Neut's scheme, respectively, to finite-difference solutions for sources at the focusing points. For the simple model with two high velocity zones it is clear that both iterative schemes successfully recovered the kinematics of the redatumed Green's function.

On the other hand, Figures 10(a), 10(b), 11(a) and 11(b) demonstrate that the neither scheme correctly recovers the dynamics when the velocity at the focusing point is different from that at the source point,  $c(x_f) \neq c(x_s)$ . This effect is a consequence of the scaling of the source strength with the source velocity.

### Marmousi vertical profile

Figures 12 to 14 compare the results of both iterative schemes for the vertical velocity profile of the Marmousi model to the corresponding FD solutions. Overall, we see a very good match of the recovered focusing functions (without any knowledge of the velocity model) and the modeled Green's functions. Particularly, we observe almost perfect kinematics, while the dynamics are wrong by a constant scale factor, caused by wrong source scaling where  $c(x_f) \neq c(x_s)$ .

The blue arrows in Figures 12(a), 12(c), 13(a), 13(c), 14(a) and 14(c) indicate event locations where the differences between the results of the two iterative schemes are more visible. We can conclude from these figures that Brogini and Snieder's algorithm is somewhat more susceptible to generating spurious noise. This noise is caused by small phase-shifts when the direct wave is subtracted from the recorded data in order to determine the reflection response. We note that these spurious events tend to grow in amplitude as the focusing time increases, probably because the amplitudes tend to decrease as the wave scatters through the velocity model. The spurious noise produced during the iterative process propagates in every iteration and can introduce artifacts, as indicated by green arrows in Figures 13(b) and 14(a), or even cancel out some events, as indicated by brown arrows in Figures 12(d) and 14(d).

Another effect that can be observed in the results from our numerical experiments is the presence of acausal events, indicated by magenta arrows in Figures 13 and 14. Note that these acausal events appear at positive time, arriving as precursors just before the direct wave. Note that the causal part of a propagating wave with source at  $x_f$ , observed at  $x_g$  (in these experiments, the receiver was located at  $x_g = 0$  km) will not arrive before the focusing time  $t_f$ . Again these spurious events tend to be more prominent as the focusing time increases. Overall, we conclude that both iterative schemes suffer the more from spurious noise the more the focusing time increases.

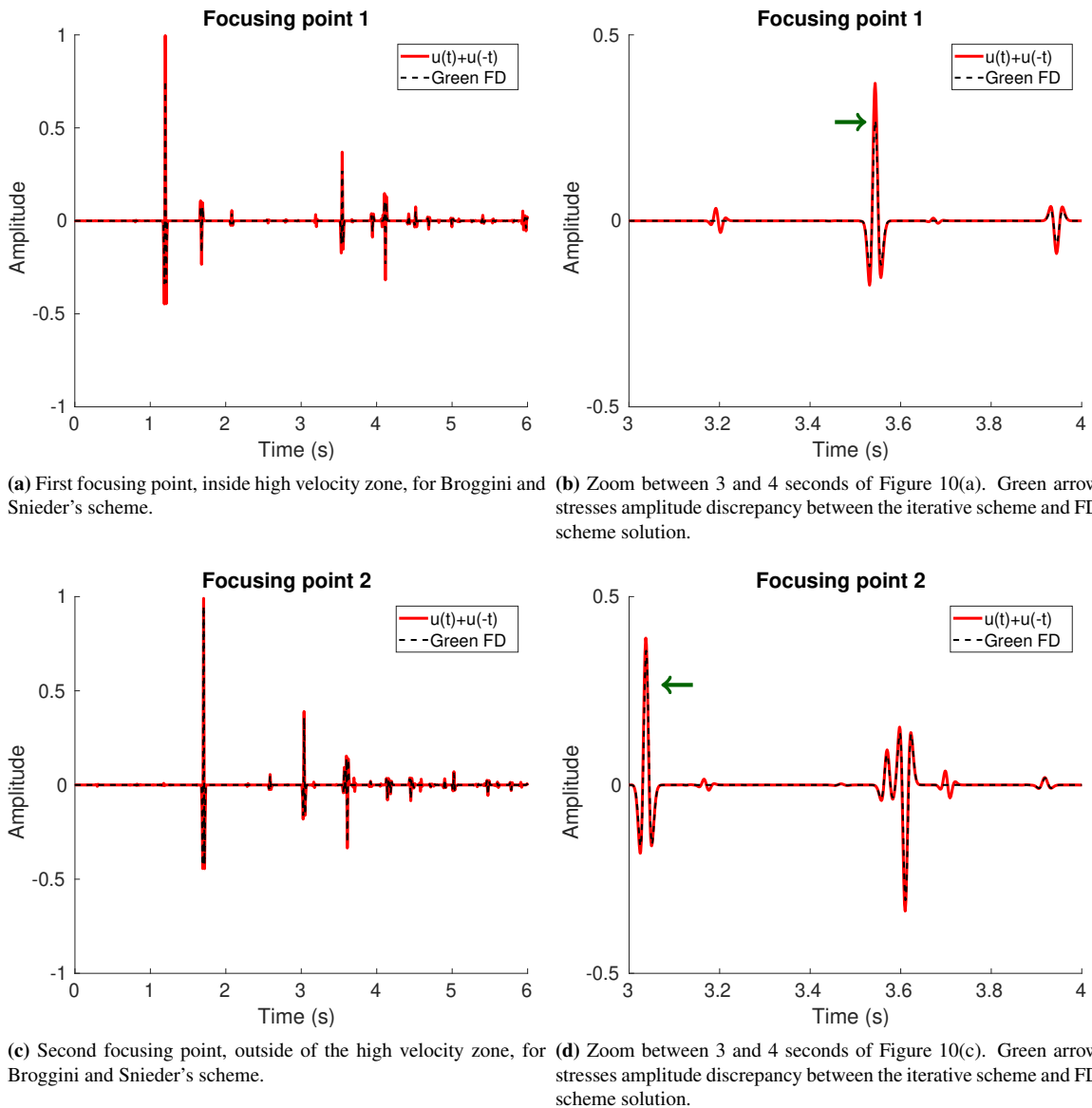


**Figure 10:** Brogini and Snieder's and FD Green's function reference solution for the two chosen focusing points in the two high velocity zone model (Figure 9(a)).

## CONCLUSION

Two slightly different iterative algorithms for solving the 1D Marchenko equation to construct the Green's function for a point source at an arbitrary focusing point have been proposed in the literature. In this work, we have investigated these two procedures theoretically and numerically. Our careful implementations have demonstrated that both algorithms can recover very good approximations of the Green's functions at the focusing point.

However, we note that, while kinematically equivalent, these algorithms lead not to fully identical results. The algorithm of Brogini and Snieder (2012) is somewhat faster than the one of van der Neut et al. (2015), because the latter needs two wavefield propagations per iteration instead of a single one. However, it allows only the construction of the complete Green's function, where van der Neut's algorithm allows for the separate calculation of the up and downgoing components. Both algorithms suffer from some the generation of some spurious events that increase for larger focusing times. Since the spurious

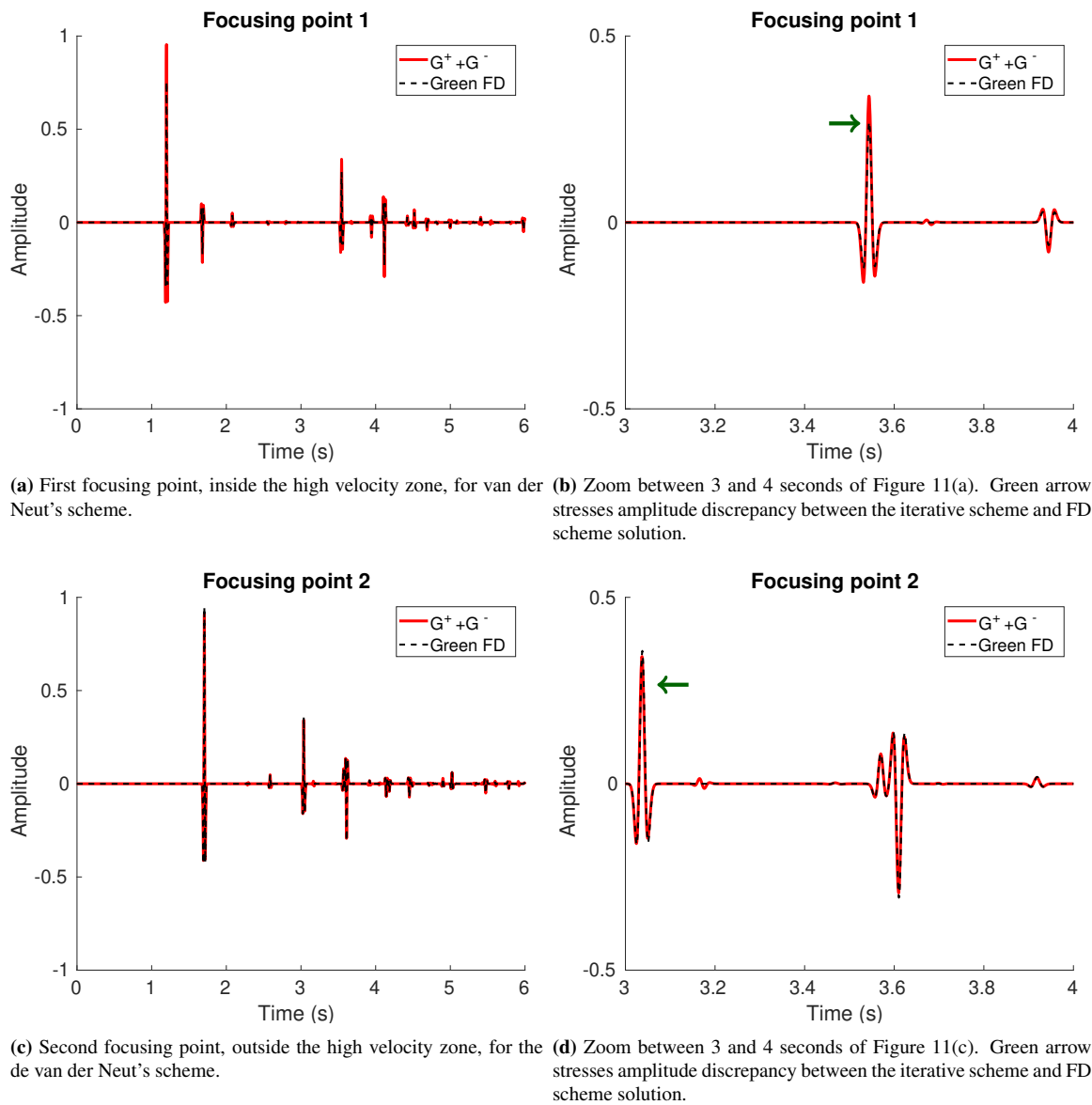


**Figure 11:** van der Neut's and FD Green's function reference solution for the two chosen focusing points in the two high velocity zone model (Figure 9(a)).

events generated by the two algorithms are different, a possible way to reduce their influence is to sum the two results.

#### ACKNOWLEDGMENTS

This work was kindly supported by the Brazilian research council CNPq, as well as by Petrobras through the Human Resource Project PRH-PB230 and a research project on seismic interferometry. Additional support for the authors was provided by the sponsors of the *Wave Inversion Technology (WIT) Consortium*, Hamburg, Germany.

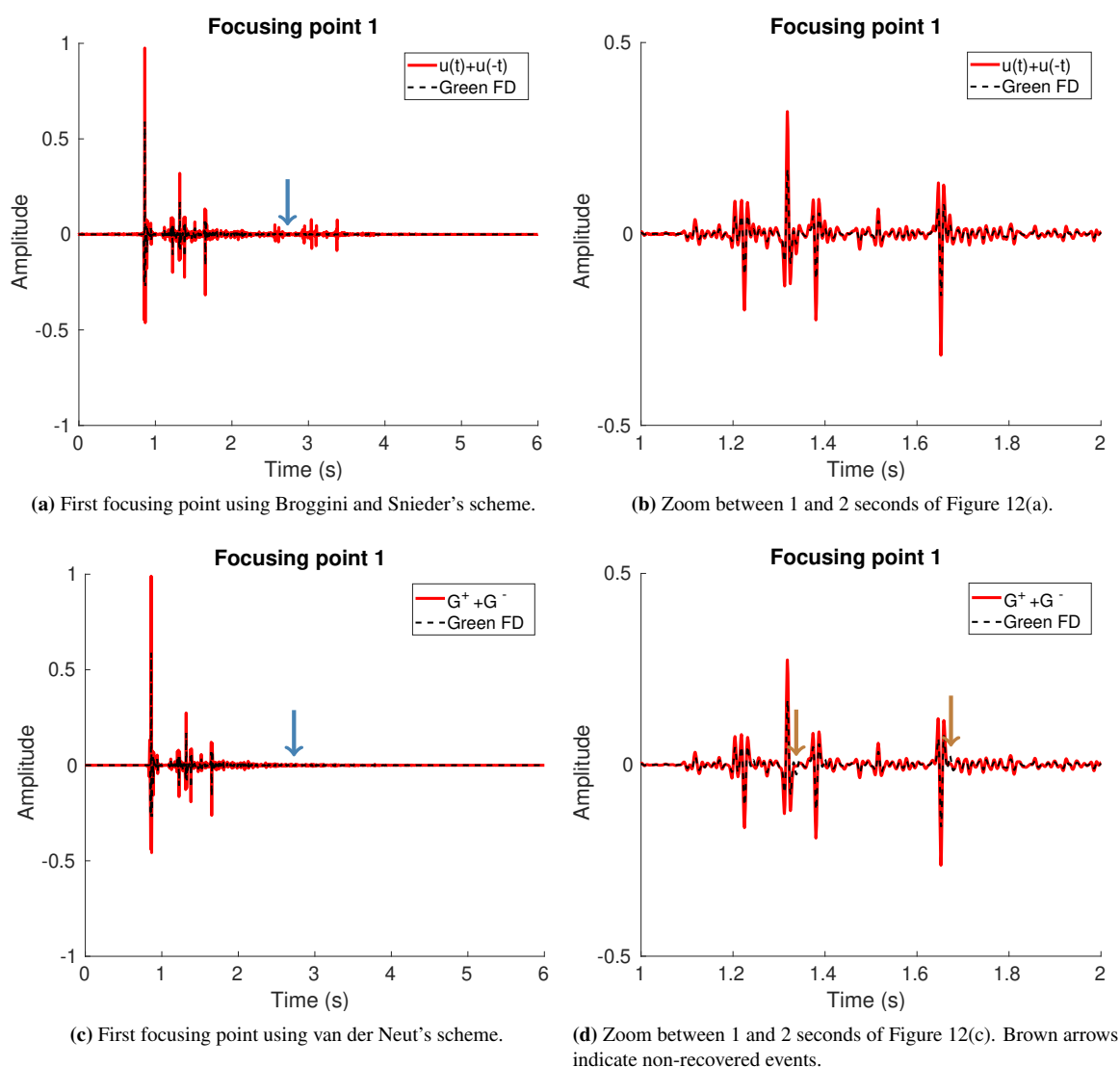


**Figure 12:** Iterative solution of the two iterative schemes for focusing point 1 in the Marmousi vertical profile (Figure 9(b)).

## REFERENCES

- Aktosun, T. (1987). Marchenko inversion for perturbations: I. *Inverse Problems*, 3(4):523–553. DOI: 10.1088/0266-5611/3/4/006.
- Bleistein, N., Cohen, J. K., and Stockwell Jr., J. W. (2001). *Mathematics of Multidimensional Seismic Imaging, Migration, and Inversion*. Springer, New York.
- Brogini, F. and Snieder, R. (2012). Connection of scattering principles: a visual and mathematical tour. *European Journal of Physics*, 33(3):593–613. DOI: 10.1088/0143-0807/33/3/593.
- Burridge, R. (1980). The Gelfand-Levitan, the Marchenko, and the Gopinath-Sondhi integral equations of inverse scattering theory, regarded in the context of inverse impulse-response problems. *Wave Motion*, 2(4):305–323. DOI: 10.1016/0165-2125(80)90011-6.
- Cui, T., Vasconcelos, I., van Manen, D.-J., and Wapenaar, K. (2018). A tour of Marchenko redatuming: Focusing the subsurface wavefield. *The Leading Edge*, 37(1):67a1–67a6. DOI: 10.1190/tle37010067a1.1.

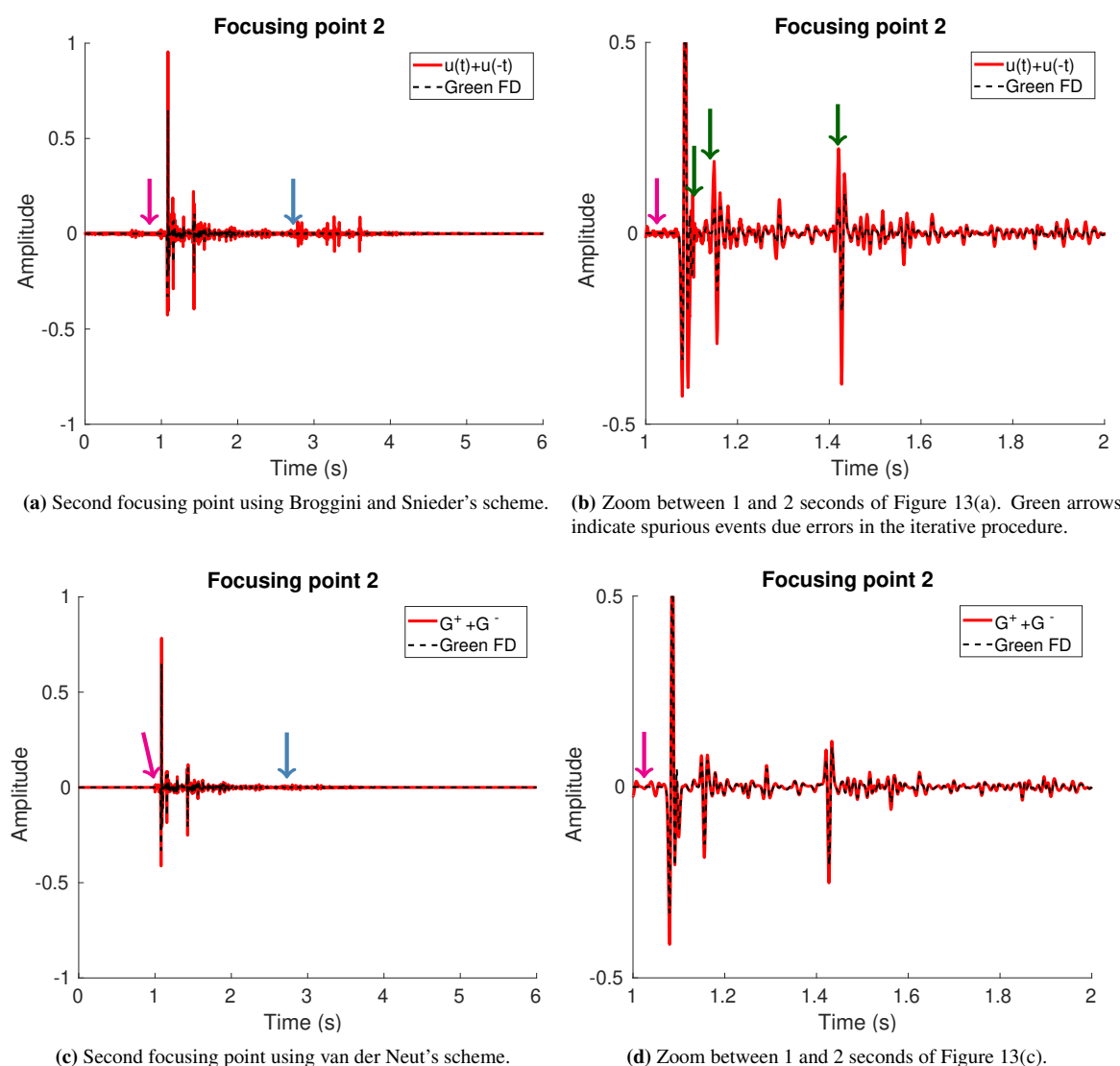


**Figure 13:** Iterative solution of the two iterative schemes for focusing point 2 in the Marmousi vertical profile (Figure 9(b)).

Lamb, G. L. (1980). *Elements of soliton theory*. Wiley & Sons, New York.

Meles, G. A., Wapenaar, K., and Curtis, A. (2016). Reconstructing the primary reflections in seismic data by Marchenko redatuming and convolutional interferometry. *Geophysics*, 81(2):Q15–Q26. DOI: 10.1190/geo2015-0377.1.

Meles, G. A., Wapenaar, K., and Thorbecke, J. (2018). Virtual plane-wave imaging via Marchenko redatuming. *Geophysical Journal International*, 214(1):508–519. DOI: 10.1093/gji/ggy143.

Mildner, C., Broggini, F., Robertsson, J. O. A., van Manen, D.-J., and Greenhalgh, S. (2017). Target-oriented velocity analysis using Marchenko-redatumed data. *Geophysics*, 82(2):R75–R86. DOI: 10.1190/geo2016-0280.1.

Rose, J. H. (2002). Single-sided autofocusing of sound in layered materials. *Inverse Problems*, 18(6):1923–1934. DOI: 10.1088/0266-5611/18/6/329.

Semih, D. (2018). Marchenko inversion. Master's thesis, Delft University of Technology.

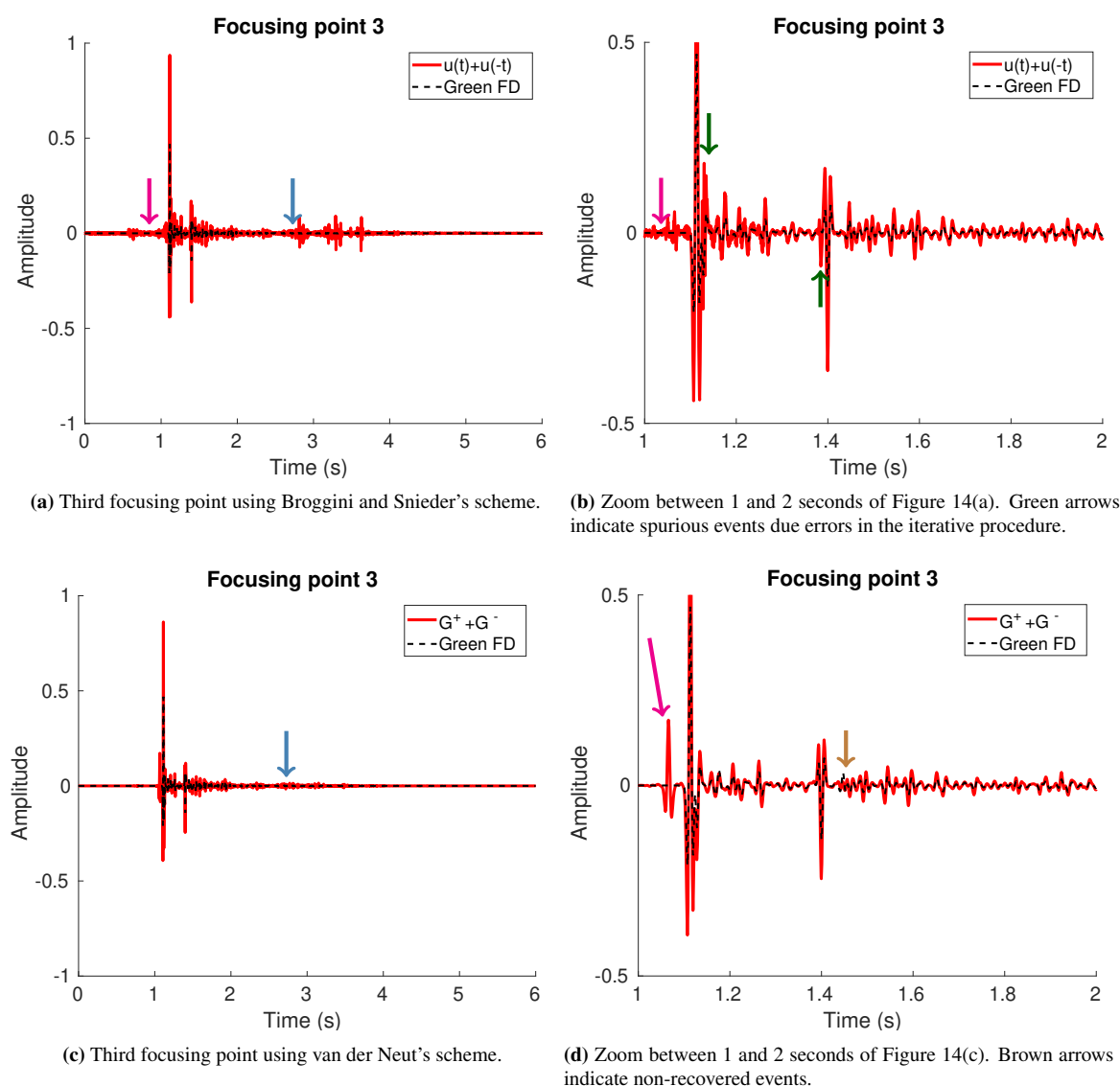


**Figure 14:** Iterative solution of the two iterative schemes for focusing point 3 in the Marmousi vertical profile (Figure 9(b)).

Singh, S., Snieder, R., Behura, J., van der Neut, J., Wapenaar, K., and Slob, E. (2015). Marchenko imaging: Imaging with primaries, internal multiples, and free-surface multiples. *Geophysics*, 80(5):S165–S174. DOI: 10.1190/geo2014-0494.1.

van der Neut, J., Vasconcelos, I., and Wapenaar, K. (2015). On Green's function retrieval by iterative substitution of the coupled Marchenko equations. *Geophysical Journal International*, 203(2):792–813. DOI: 10.1093/gji/ggv330.

Wapenaar, K., Brogini, F., Slob, E., and Snieder, R. (2013). Three-dimensional single-sided Marchenko inverse scattering, data-driven focusing, Green's function retrieval, and their mutual relations. *Physical Review Letters*, 110(8). DOI: 10.1103/physrevlett.110.084301.

Wapenaar, K., Thorbecke, J., van der Neut, J., Brogini, F., Slob, E., and Snieder, R. (2014). Marchenko imaging. *Geophysics*, 79(3):WA39–WA57. DOI: 10.1190/geo2013-0302.1.